EXPERIMENTAL STUDY ON INTERFERENCE FLOW OF A SUPERSONIC BUSEMANN BIPLANE USING PRESSURE-SENSITIVE PAINT TECHNIQUE

Hiroki Nagai*, Soshi Oyama*, Toshiyuki Ogawa, Naoshi Kuratani**, Keisuke Asai***
*** Department of Aerospace Engineering, Tohoku University, Sendai, Japan**
**** Institute of Fluid Science, Tohoku University, Sendai, Japan**

Keywords: *Busemann biplane, Pressure-Sensitive Paint, Shock interference*

Abstract

Using Pressure Sensitive Paint, the pressure distributions on thin wings of the Busemann biplane model were measured in the small supersonic indraft wind tunnel. The observed phenomenon is so complicated that it is completely different from the prediction of the simple two-dimensional theory. Referring to Schlieren photograph and CFD analysis, it is found that these complex pressure fields are caused by the shock wave generated downstream just behind the wing ridge line. The results of this experiment show that the interference between Busemann biplane wings is sensitive to a small change in flow condition. A care must be taken in a wind tunnel test to realize the design condition of Busemann biplane where the shock waves are completely cancelled with each other.

1 Introduction

The generation of shock waves is one of the fundamental impediments to realize commercial transport aircraft. In supersonic flight, the airplane generates sonic boom that causes noise damage on the ground and wave drag that increases operating cost. Busemann proposed in 1935 a novel concept to reduce wave drag using the interference of two airfoils arranged in a biplane configuration [1], [2]. This biplane consists of two identical wings shaped like a half cut of the diamond airfoil, placed in such a way that the convex parts of the wings are set up face-to-face, shown in Fig.1. In a usual airfoil, the compression wave is generated from the leading edge of the wing. On the other hand, in Busemann biplane, the compression waves generated from the two wings are counterbalanced to the expansion waves generated from the convex parts of the wings. As a result, the shock waves are not transmitted outside of the biplane and the wave drag due to airfoil thickness is significantly reduced.

This concept has been long considered impractical, but, due to an advancement of CFD technology, an interest in Busemann biplane has been revived and the feasibility of the biplane configuration for supersonic flight have been studied by many researchers [2],[4],[5],[6]. However, these studies are based mainly on CFD calculations and not validated by experiment so that a discussion on the wave cancellation mechanism between the two wings is very limited.

The objective of this research is to measure the wing surface pressure distribution on a Busemann biplane and to study the two-dimensional interference phenomenon between the two wings. Since the Busemann biplane

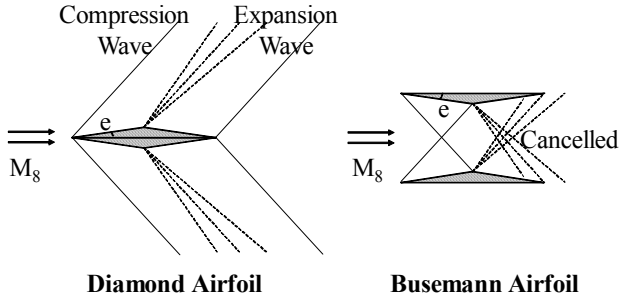

Fig.1 Concept of Busemann Biplane

wings are so thin (the wing thickness ratio is 0.05) that it is difficult to install static pressure taps on the model. In this experiment, we used Pressure-Sensitive Paint (PSP) to measure surface pressure distributions on the model. PSP is an optical pressure measurement technique based on photochemical reaction called “oxygen quenching”. This is a coating type sensor and considered only means to measure pressure fields on a thin airfoil model. In this study, wind tunnel experiment was conducted in a 60mm x 60mm indraft supersonic wind tunnel. The centerline pressure distribution obtained using PSP were compared with two-dimensional theory. Referring to the Schlieren photographs and CFD calculation, the complicated three-dimensional interference phenomenon between the two wings, including shock wave/boundary layer interactions were analyzed. On the basis of these experimental results, the wave cancellation mechanism of the Busemann biplane is discussed.

2 Experimental Setup

2.1 Wind Tunnel

The 60mm x 60mm indraft supersonic wind tunnel consists of an intake/nozzle section, a convergent-divergent supersonic nozzle, a test section, a diffuser with a manual opening valve, and a dump tank. The supersonic nozzle is connected to a 220-mm-long test section that maintains supersonic flow along its entire length [7]. A shape of the supersonic nozzle was a calculated by a method of characteristics with a correction for boundary layer thickness. The free-stream Mach number is 1.69±0.01. Flow duration is about 15 second.

Figure 2 shows the overall of the wind tunnel and the flow channel with the front sidewall removed. Both sidewalls are made of 30-mm-thick aluminum plate with a turntable. The turntable is used to mount the model. For Schlieren measurement, the turntables made by acrylic material were used on both sides. On the other hand, for PSP measurement, the aluminum turntable was set on one side wall to change an attack angle of the model.

The angle of attack was set at 0 deg (design point), 2 deg, and 4 deg. The angle of attack was increased further to see when the flow between the two wings was choked. When starting the tunnel, it is usual that choking occurs between the two airfoils [8]. Therefore, it is necessary to start the Busemann wing from a Mach number higher than the design value to prevent choking.

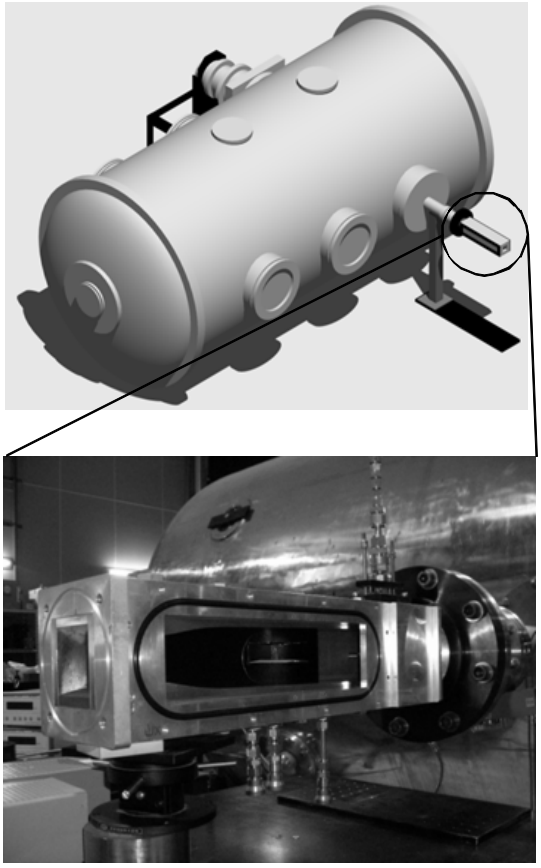

Photo of Test Section (Sidewall removed)

Fig.2 Photo of the overall of the wind tunnel and the flow channel with the front sidewall removed.

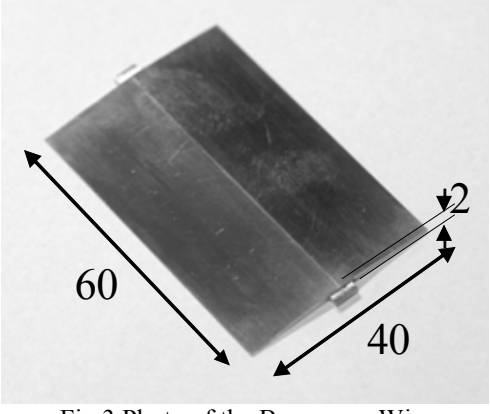

Fig.3 Photo of the Busemann Wing

In the present experiment, Free-stream Mach number was changed from higher to the design Mach number gradually by opening a plate covering the tunnel intake manually. By using this method, occurrence of choked-flow and hysteresis of Busemann biplane could be avoided. The time required to open the intake completely is about seven seconds, so available test time was about five seconds.

2.2 Test Model

In this experiment, we used two types of models. One is a biplane which is an original Busemann biplane and another one is a single-plane airfoil (Fig.3). The single-plane airfoil is actually one of the two airfoils of the biplane model. The chord length is 40 mm, the span length is 60 mm, and thickness is 2 mm. So, the aspect ratio is 1.5, the thickness to chord ratio is 0.05, and a wedge angle is 5.71 degrees. The wings are made of stainless steel, and machined by wire cutting. PSP were applied using ordinary air brush over the white base coat and FIB base coat (FB-200, Innovative Scientific Solutions, Inc. (ISSI)) applied beforehand. Ten black markers for image registration were painted on a top surface of the model.

2.3 PSP Formulation

PSP is a coating-type sensor that consists of luminescent molecules and polymer binder, shown in Fig.4. Figure 5 shows the Jablonski energy-level diagram. The sensor molecules in PSP are excited electronically to an elevated energy state, when illuminated with light at an appropriate wavelength. The excited PSP molecules return to the ground state through several photochemical mechanisms; radiative decay (luminescence), non radiative decay (release of heat) and oxygen quenching. The principle of PSP is based on oxygen quenching. In the presence of oxygen molecules, the excited energy of sensor molecules is transferred to oxygen molecules, so that no luminescence is emitted. As a result, the luminescence intensity is reduced with increasing oxygen concentration or, in other words, oxygen partial pressure that is proportional to air pressure. The luminescence intensity of PSP is influenced by temperature. The effect of temperature must be corrected to measure pressure quantitatively.

Theoretically, the relationship of the luminescence intensity I and the pressure P is expressed by the following relation, known as Stern-Volmer relation.

$$\frac{I(P_{ref},T)}{I(P,T)} = A(T) + B(T)\frac{P}{P_{ref}} \qquad (1)$$

where the subscript ref represents the reference conditions, and $A(T)$ and $B(T)$ are calibration coefficients. Note that these coefficients are functions of temperature T. Using Eq.(1), the surface pressure P can be calculated from the ratio of luminescence intensity images between the wind-on and wind-off (reference) conditions.

For actual conditions, however, temperature at the wind-on condition (T) is different from that at the wind-off condition (T_{ref}). Since PSP is dependant not only on pressure but also on temperature, it is necessary to correct the effect of temperature to calculate

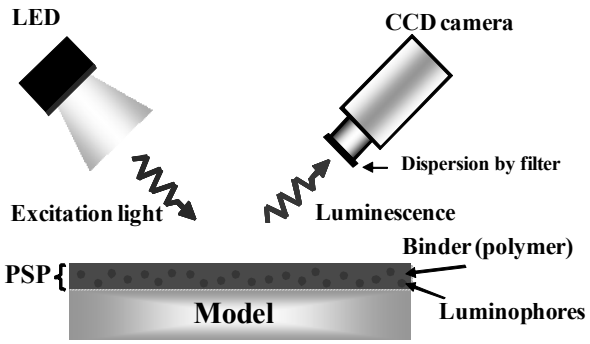

Fig.4 Schematic illustration of PSP measurement.

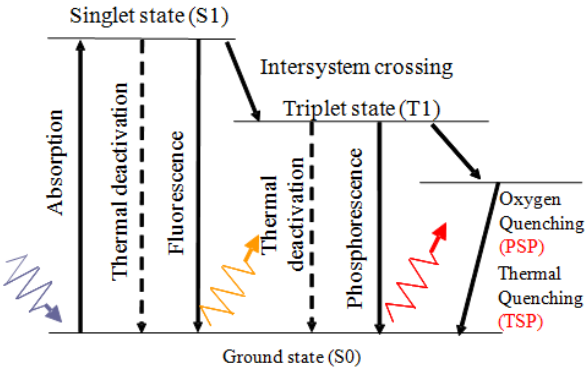

Fig.5 Jablonski energy-level diagram.

surface pressure. In this study, we use Eq.(1) transformed to the following expression [3].

$$\frac{I(P_{ref},T_{ref})}{I(P,T)} = \alpha(T)\cdot\left(A(T)+B(T)\frac{P}{P_{ref}}\right) \quad (2)$$

where $\alpha(T)= I(P_{ref}, T_{ref})/I(P_{ref}, T)$. We call this factor as the temperature correction factor.

In this experiment, UF470, product of ISSI, is used as PSP. The composition of the PSP is as follows.

- Luminophore: PtTFPP
- Binder: FIB
- Solvent: Benzene
- Scattering agent: TiO_2

This paint emits the phosphorescence with a peak wavelength of 650nm, when excited by 405nm light. The characteristic of UF470 is "ideal", that means the coefficients A and B are independent of temperature. Therefore, for UF470 paint, only the effect of temperature on α in Eq.(2) should be taken into account. The Stern-Volmer relationship of this paint is shown in Fig.4.

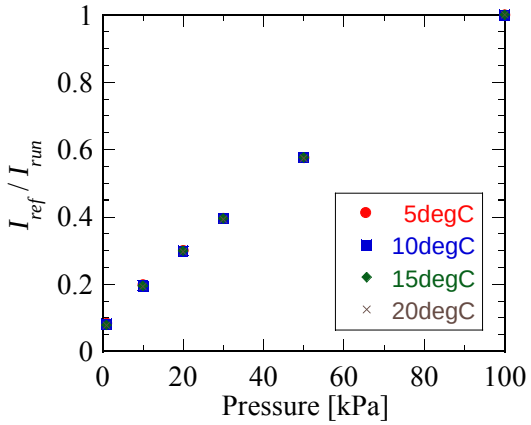

Fig.4 Stern-volmer relationship.

2.4 Optical Setup

A schematic and a photograph of optical setup are shown in Fig.6. For PSP measurement, the excitation light source was two UV-LED units of which peak wavelength is 395nm. To

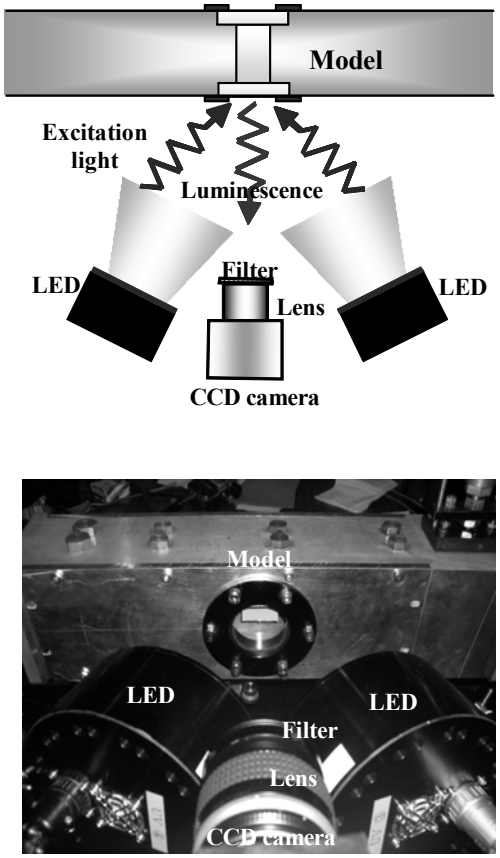

Fig.6 Schematic illustration of PSP measurement and photo of optical setup.

cut undesirable near infrared component of excitation light, a "band-passed filter" which could transmit light at the wave length of 400±50 nm was placed in front of the illumination unit. The same excitation light source was used for both PSP and TSP tests.

Luminescent intensity image was acquired using a 12bit cooled CCD camera (Hamamatsu, C4742-95-12NR). The spatial resolution of this camera was 1024×1024 pixels. Either of a band-passed filter, which could be made to pass the wave length of 650±20 nm, or a high-pass filter, which could be made to pass the wave length of over 580nm, was placed in front of the camera lens for PSP and TSP measurements, respectively, to cut the excitation lights from LEDs.

In the interval, a sequential 70 wind-on images were taken during flow duration, the exposure time of one shot is 359 msec.

2.5 Data Processing

Just before the wind tunnel starts, the wind-off reference image I_{ref} was taken. Five images were acquired as the reference images and averaged to reduce shot noise and read-out noise. A sequential 70 wind-on images were taken during flow duration. These wind-on images can divide into three categories; first the images taken during the starting process, secondly the images taken after the flow is completely started, and finally the images taken after the tunnel is shut down. Here we call the image just before the tunnel stops, I_{run}, and the image just after the tunnel stops I_{ref_after}. Both of the wind-off images and the wind-on images were compensated for dark images.

For PSP measurement, we use I_{ref_after} as the reference image, because this method can reduce the influence of temperature, according to Yamashita et al (2006) [3], when the temperature distribution at the wind-on condition is preserved immediately after the tunnel is shut down. We have confirmed from Temperature Sensitive Paint test results that this is the case for this wind tunnel experiment.

The PSP images were processed through a sequence of the following steps:

1. Ensemble averaging of five images
2. Subtraction of dark images
3. Registration of the wind-on and wind-off images
4. Calculation of luminescence intensity ratio
5. Calculation of pressure and temperature using a-priori method. The coefficients were obtained using a calibration chamber and paint samples.
6. Correction of temperature by multiplying the temperature correction factor $\alpha(T)$, calculated from temperature measured by a thermocouple.

3 Results and Discussions

3.1 PSP for α=0 deg, biplane configuration

Figure 7 shows a pressure map of the upper surface of the lower wing of the Busemann biplane by using PSP (Case A). Figure 8 shows the pressure distributions along the span direction of y/w=0.1, 0.3, 0.5. Attack angle was 0 degree. The flow runs from the left to the right. The color indicates an absolute pressure as shown by the color bar from 10 k*Pa* to 40 k*Pa*. In this experiment, air pressure was 101.5 k*Pa*, air temperature was 22.5 *degC*, A focal length of the camera was 35 mm, and lens aperture was F=8, and an exposure time was 359 msec.

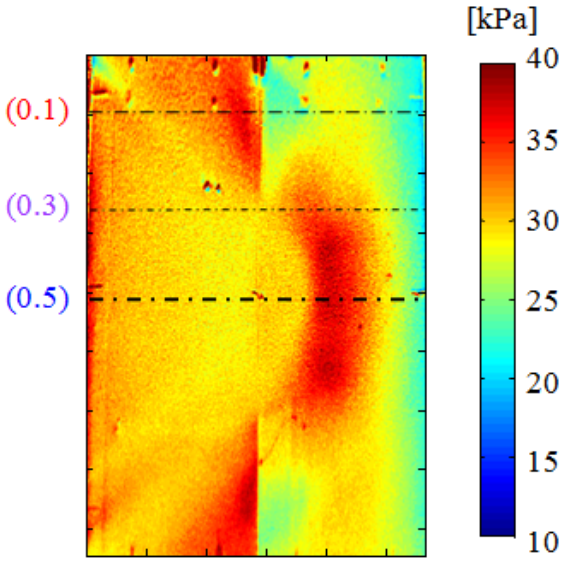

Fig.7 Pressure map of the upper surface of the lower wing of the Busemann biplane.

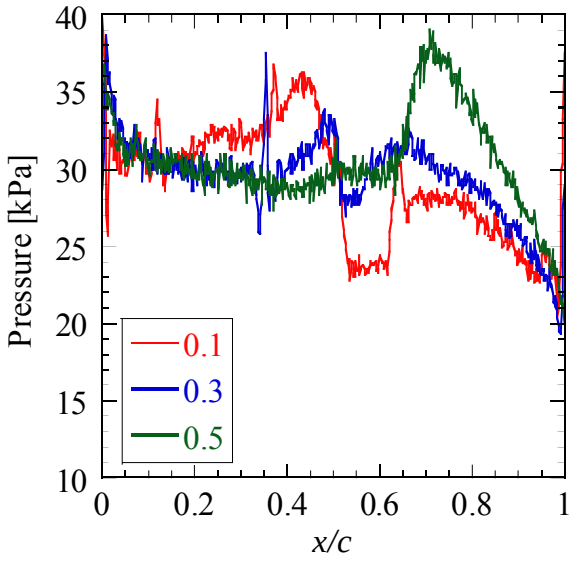

Fig.8 Pressure distributions along the span direction of y/w=0.1, 0.3, 0.5.

Since the airfoils of Busemann biplane are so thin, it is difficult to capture pressure distribution on the model using static hole. But, using PSP, the pressure distribution on the model was clearly visualized. The observed phenomenon is so complicated that it is completely different from that predicted by a simple two-dimensional theory. This indicates that some three-dimension mechanism was involved in this phenomenon. The areas suggesting the three-dimensional effects were enlarged from the junction between the wing leading edge and the wall to the center line of the wing, showing the disturbance caused by the interaction at the junction is propagated downstream. It is also noted that abrupt pressure increase was observed at the center of the downstream wing surface. This unexpected high pressure area appeared behind the ridge line is different from the theory. This phenomenon will be discussed in the later section.

3.2 PSP for α=0 deg, single-plane configuration

Fig.9 shows a pressure distribution of the upper surface of the lower wing of the single-plane configuration by using PSP (Case B). Attack angle was 0 degree. In this experiment, air pressure was 101.5 k*Pa*, and air temperature was 22.5 *degC*. Other conditions were the same as Case A.

It is seen in Fig. 9, for the single-plane configuration, the observed flow is similar to the theory. This is contrary to the case of biplane, where the flow structure was so complicated. It means that the complexity of biplane flow is attributed to the interference between the upper and lower wings. Figure 10 compares the centerline pressure distribution between biplane and single-plane cases. It is noted in Fig. 10 that the pressure on the upstream surface decreases gradually in both biplane and single-plane cases. This trend can be due to an influence of boundary layer evolution. The present experiment was conducted at relatively low Reynolds number and so it is considered that the effect of boundary layer thickness appeared as gradual expansion along the upstream surface.

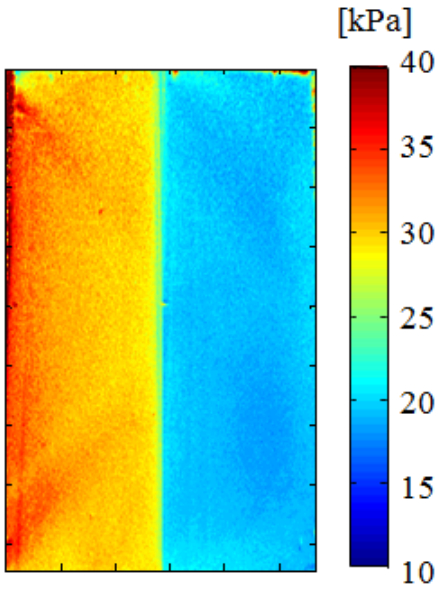

Fig.9 Pressure map of the upper surface of the lower wing of the single-plane.

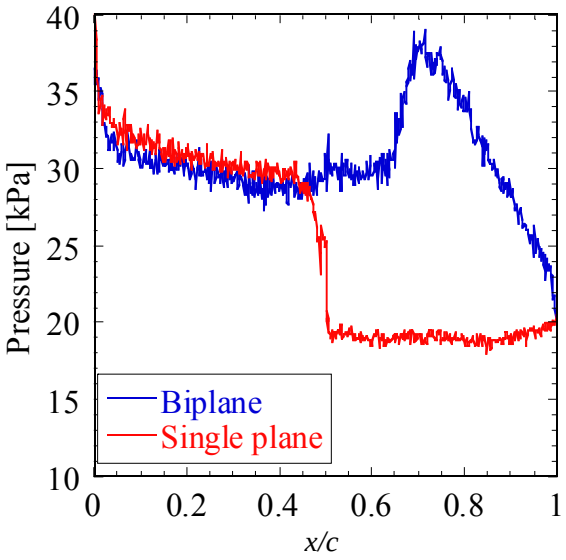

Fig.10 Comparison of Pressure distributions along the centerline of single-plane with bi-plane.

3.3 Schlieren Photograph for α=0 deg, biplane configuration

Figure 11 shows Schlieren images taken during the starting process. In this experience, the wind tunnel condition was the same as Case A and Case B. It is seen in this figure that, at the leading-edge, compression waves are generated

not only inside the biplane but also outside of the biplane, although the attack angle is set at 0 degree. This is probably due to the effects of the boundary layer thickness evolution from the leading-edge. From Fig, 11, it is seen that the shock waves inside the biplane interfere with expansion waves and almost cancelled immediately before the tunnel intake is completely opened. On the other hand, after the intake is fully opened, the cancellation of the shock waves by expansion waves was not performed completely, and a shock wave and following subsonic-speed region appeared between the upper and lower wings downstream of the model ridge line.

Figures 12 (a) and (b) shows the images of pressure distribution calculated by CFD (two-dimensional) for α=0 deg, biplane configuration. The Euler code was used in the calculation, so that the influence of viscosity has not been taken into consideration.

Figure 12 (a) shows the case for Mach number of 1.69 (design value of our model). On the other hand, Fig. 12 (b) shows the case for Mach number of 1.64, which corresponds to the state immediately before choking, is occurred. It is seen that, at M=1.70, shock waves are almost canceled as predicted by the simple theory. In contrast, at M=1.64, a sufficient cancellation of the shock wave by interference with expansion waves is not performed, and a subsonic region appeared between the upper and lower wings. This is similar to the Schlieren picture in Fig. 11. It can be said that the phenomenon similar to the CFD calculation for M=1.64 happened in our experiment.

This fact indicates that the high pressure area in case A is related to the appearance of a shock wave down stream of the wing ridge line. Several possible mechanisms can be thought about as a cause of this phenomenon. One is a decrease of Mach number, but the Mach number determined by calibration is 1.69±0.01 so it is not the cause of the observed phenomena. The second possibility is an influence of the boundary layer. Reynolds number is 1.5×10^5 at that the boundary layer becomes fairly thick so that the design condition could be changed. Finally, an error of the model shape could also be a cause of the observed phenomena. Since manufacturing tolerance required to the present model is very small, it is difficult to make a model to match the designed values. From these

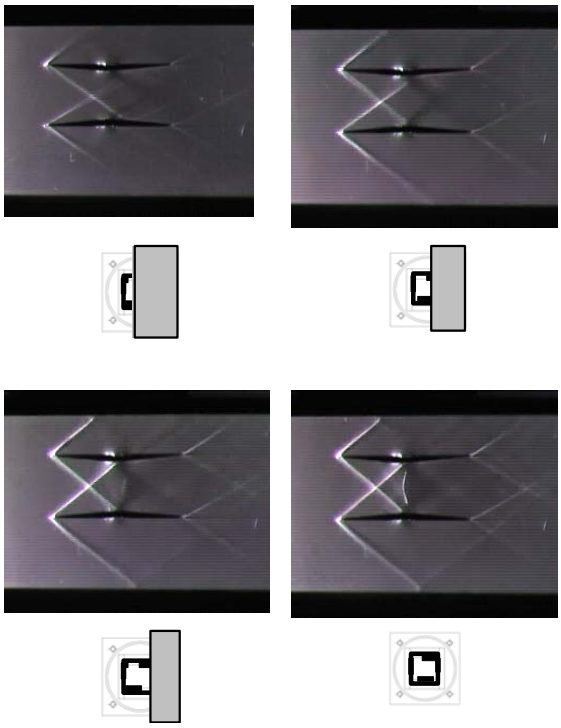

Fig.11 Schlieren pictures taken during the starting process of Busemann biplane.

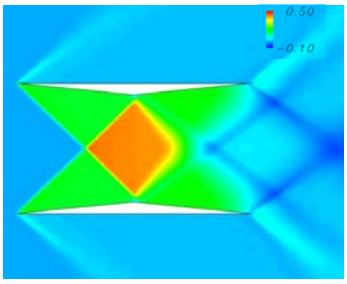

(a) M=1.69

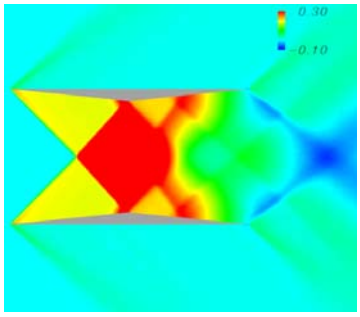

(b) M=1.64

Fig.12 CFD results of pressure Cp distributions calculated by Maruyama[4].

considerations, it can be concluded that the phenomenon observed in Fig. 11 is not caused by a decrease of Mach number, but by an influence of the boundary layer and a small difference from the designed shape. In any case, it is noted that the observed phenomenon is very sensitive to small change in the test condition.

3.3 Influence of attack angle on PSP images

Figure 13 compare the results of pressure distribution of the upper surface of the lower wing measured by using PSP for various attack angles. In these tests, an angle of attack was changed from -2, 0, 2, 4 degrees. The data for -2 degrees can be regarded as the data of the lower surface of the upper wing for +2 degrees. Figure 14 shows centerline pressure profiles extracted from the PSP images in Fig. 13.

Figures 13 and 14 show that the pressure along the centerline where the flow two-dimensionality is being kept decreases as the attack angle increases. This trend corresponds to movement of diagonal shock wave system predicted by the simple theory. At the attack angle of 4 degrees, the pressure on the upstream surface increased rapidly, indicating a resultant drag penalty is increased. It is seen in Fig. 13, that the high pressure region is observed downstream of the wing ridge line for attach angle of 2 and 4 degrees too. It is considered that this phenomenon is caused by the same mechanism as the case for 0 degree. It is noted that, in the pressure profile for 2 and 4 degree, there are a step of pressure in the middle of the upstream surface. This step move forward gradually with increasing the angle of attack. This step does not exist on the single-plane wing, so this phenomenon is not caused by the effect of temperature distribution, but by something relating to the interactions between the two wings. It is concluded that a further study is required to understand underlying flow mechanism.

7 Conclusions

The wing surface pressure distribution on a Busemann biplane was measured by Pressure Sensitive Paint and the observed the interference phenomenon between the two wings were analyzed by comparing PSP data with Schlieren pictures and CFD calculations. The conclusions obtained in this study can be summarized as follows;

1. A complicated pressure distribution was captured using PSP for a thin airfoil of

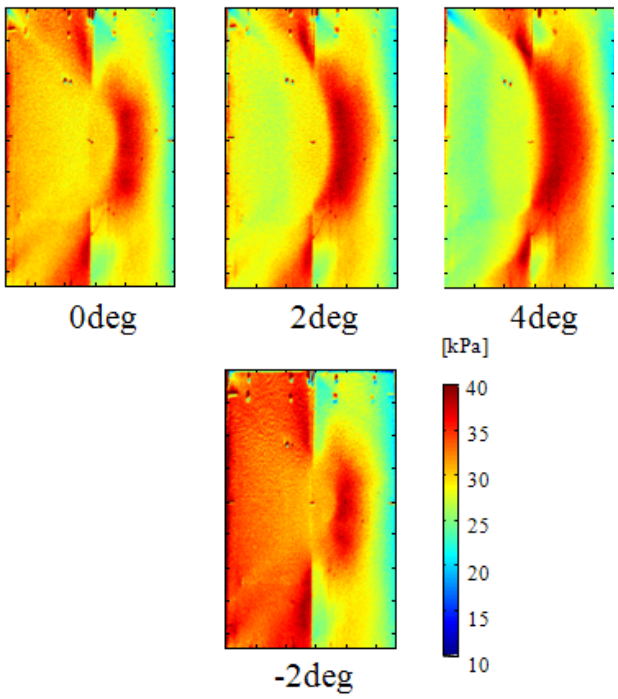

Fig.13 Pressure map of biplane for α=0, 2, 4, -2 deg,

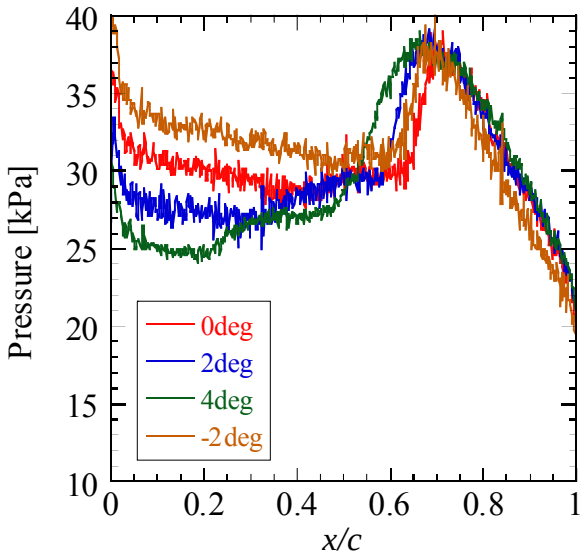

Fig.14 Pressure distributions of biplane for α=0, 2, 4, -2deg

Busemann biplane. The observed phenomenon is different from the simple theory.

2. Comparing PSP data with Schlieren photograph and CFD, it is found that a complex pressure field on the model was caused by a shock wave generated behind the ridge line.
3. The interaction of shock waves between a Busemann biplane is sensitive to a small change in test condition. A care must be taken in a wind tunnel test to realize the design condition of Busemann biplane where the shock waves are completely cancelled with each other.
4. A further study is necessary to fully understand the interacting flow mechanism of a Busemann biplane.

References

[1] H. W. Liepmann and A. Roshko, Elements of Gas Dynamics, John Wiley & Sons, Inc., New York, 1957

[2] K. Kusenose, K. Matsushima, Y. Goto, H. Yamashita, M. Yonezawa, D. Maruyama, and T. Nakano, A Fundamental Study for the Development of Boomless Supersonic Transport Aircraft, AIAA-2006-0654, 2006

[3] T. Yamashita, H. Sugiura, H. Nagai ,K. Asai and K. Ishida, Pressure-Sensitive Paint Measurement of the Flow around a Simplified Car Model, ISFV12-2006-67.4(259), 2006

[4] D. Maruyama and K. Matsushima, Aerodynamic Design of Biplane Airfoils for Low Wave Drag Supersonic Flight, AIAA-2006-3323, 2006

[5] M. Yonezawa, H. Yamashita, and S. Obayashi, Investigation of Supersonic Wing Shape Using Busemann Biplane Airfoil, AIAA-2007-686, 2007

[6] H. Yamashita, M. Yonezawa and S. Obayashi, A Study of Busemann-type Biplane for Avoiding Choked Flow, AIAA-2007-688, 2007

[7] J. Lepicovsky, T. J. Bencic and R. J. Bruckner, Application of Pressure Sensitive Paint to Confined Flow at Mach Number 2.5, AIAA-97-3214, 1997

[8] N. Kuratani, T. Ogawa, H. Yamashita, M. Yonezawa, and S. Obayashi, Experimental and Computational Fluid Dynamics Around Supersonic Biplane for Sonic-Boom Reduction, AIAA-2007-3674, 200.

Copyright Statement